



Stockholm
University

Bachelor Thesis

Degree Project in
Earth Science 15 hp

Petrological, geochemical and structural evidence of fluid-rock interaction in the Siljan Ring

William Crang



Stockholm 2024

Department of Geological Sciences
Stockholm University
SE-106 91 Stockholm

ABSTRACT

The Siljan Ring in Dalarna, Sweden is the site of the largest meteor impact crater in Europe and has long been a topic of discussion regarding methane production. However, the source of this methane and the timing of production in relation to the impact remain unclear. An outcrop of red Ordovician limestone preserved on the edge of a downfaulted zone encircling the crater's central plateau is crosscut by fractures surrounded by pale-coloured reduction haloes within which precipitates can be observed. These haloes suggest interaction with a reducing agent mobilised within a fluid flow, of which methane would be a prime candidate. A field study was subsequently undertaken to establish the reaction whereby these haloes were formed, as well as the timing of their formation relative to the Siljan impact based upon petrological, geochemical, and structural data obtained in the field. Results from this study show that a methane-bearing hydrothermal fluid mobilised within the fractures has preserved the original mineralogy of the limestone within the reaction haloes whilst the country rock beyond was being oxidised. Pyrite is shown to be preserved within the pale reaction haloes, whilst its oxidation within the country rock is shown to be the source of the limestone's distinct red colouring. Fracture and bedding orientation at the study site suggest the hydrothermal event to have been simultaneous with the meteor impact, with the fractures forming part of a wider complex network of impact features. Whilst mobilisation associated with the meteor impact is a likely cause of methane release, the exact source of the methane active at the study site is unclear.

Keywords

methane, hydrothermal fluids, fluid-rock interaction, impact craters, reduction haloes, pyrite preservation, Siljan Ring.

Contents

1. Introduction.....	4
1.1 Geology.....	4
1.2 Reduction Haloes.....	4
1.3 Methane in the Siljan Ring.....	5
1.4 Timing of hydrothermal events.....	6
Aim.....	7
2. Methodology.....	7
2.1 Structural Analysis	7
2.2 XRF Analysis.....	8
2.3 Thin Section Analysis.....	9
3. Results.....	9
3.1 Structural Analysis	9
3.2 XRF Analysis.....	13
3.3 Thin Section Analysis.....	16
3.3.1 Microscopy	16
3.3.2 Point Counting.....	20
3.3.3 Image Analysis	20
4. Discussion	22
4.1 The halo-forming reaction.....	22
4.2 Fluid chemistry	23
4.3 Timing of the hydrothermal event.....	24
4.4 Other hydrothermal events	25
4.5 Future work	25
5. Conclusion.....	25
Acknowledgements	26
References.....	26

1. Introduction

On the shore of Lake Siljan in Dalarna, Sweden, approximately 4km northwest of Rättvik, an outcrop of Ordovician red-grey limestone containing orthoceratites is cross-cut by numerous fine fractures within which precipitates can be observed (Fig. 1.1). These fractures are surrounded by pale-coloured haloes, suggesting interaction with a reducing fluid, of which a methane bearing fluid is a likely candidate. The outcrop, which forms the study site for this project, is situated within the Siljan Ring (Fig. 1.2), which with an estimated diameter of between 52 and 85km is the largest known impact structure in Europe (Reimold et al., 2005). However, the origin of methane in this area and the timing of fluid mobility within these fractures in relation to the impact event remains unclear.

1.1 Geology

The Siljan Ring consists of a central uplifted region of Svecokarelian granitic basement rock surrounded by a ringed depression of downfaulted Ordovician and Silurian sedimentary rocks, with impact breccias containing various hydrothermal minerals such as smectites, chlorite, and hematite (Hode et al., 2003; Naumov, 2005). Secondary veins in the bedrock containing quartz and calcite can be found throughout the area (Komor et al., 1988). Further evidence of the meteorite impact is seen in examples of shock metamorphism, including planar deformation features in quartz, shatter cones, and veins bearing fine-grained, glassy, pseudotachylites (Komor et al., 1988; Reimold et al., 2005). The Siljan impact has been isotopically dated to 380.9 ± 4.6 Ma using the argon–argon ($^{40}\text{Ar}/^{39}\text{Ar}$) method on the impact breccias in its central plateau, placing it in the Upper Devonian epoch (Jourdan et al., 2012). The region lies just to the east of the Caledonide mountain belt, formed prior to the impact in various stages between 510 and 400 Ma as a result of continental collision between Baltica and Laurentia, and of which evidence can be found in the stratigraphic column recovered from some parts of the ring (Fredén, 1994; Lehnert et al., 2013).

1.2 Reduction Haloes

Reduction haloes are a common feature in red beds, including limestones found in Sweden, and are caused by the ferric oxide which gives the rocks their distinct colour being chemically reduced, and its oxygen consumed by a reducing agent (Schmitz et al., 2016; McMahan et al., 2018). The molecular structure of methane means it is particularly suited to this role in redox reactions and is even utilised industrially for this purpose as it produces less CO_2 (Alizadeh et al., 2009). Iron has also been shown to act as a viable electron receptor in the anaerobic oxidation of methane, particularly from microbially produced sources (Beal et al., 2009; Bar-Or et al., 2017). A redox reaction involving the

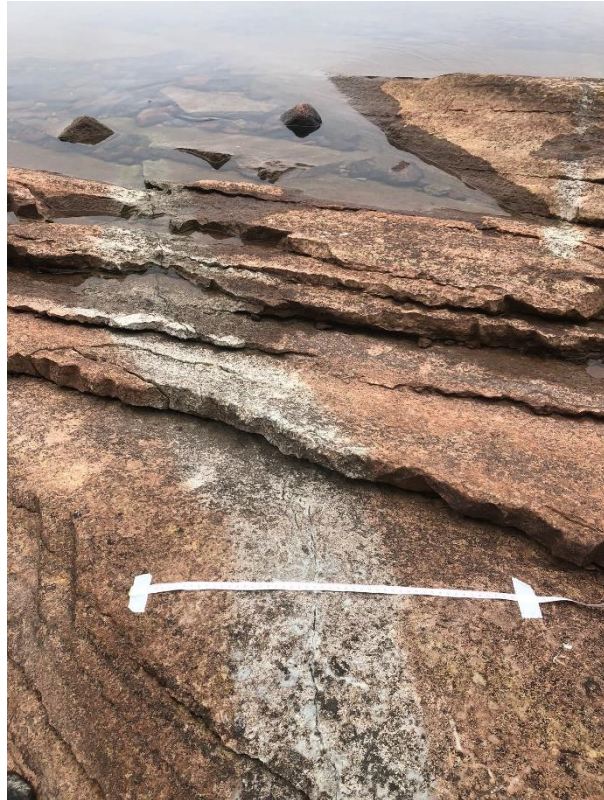


Figure 1.1. Example of the fractures and accompanying reaction haloes seen at the study site. The tape measure is extended to approximately 45cm.

iron oxide and methane is therefore seen as a possible explanation for the haloes seen at the study site.

An alternative to this hypothesis is that rather than a reducing agent altering the mineralogy of the limestone within the halo, it may actually have preserved it. Evidence exists from localities in Greece of haloes surrounding shear zone fractures preserving carbonate-bearing blueschist facies mineral assemblages, despite greenschist facies conditions, due to interaction with a CO₂-bearing fluid (Kleine et al., 2014). Whilst the geological setting and mineralogy involved are different to the Siljan site, the potential for a fluid flow to preserve a mineralogy rather than alter it presents this as another possible explanation for halo formation.

1.3 Methane in the Siljan Ring

Potential methane reserves within the Siljan Ring were first proposed following arguments made by the astrophysicist Thomas Gold (Gold & Soter, 1980), who theorised that impact-deformed basement rocks might contain reserves of mantle derived hydrocarbons, such as abiogenic methane, which could have risen upwards through impact generated fractures and accumulated in reservoirs near the surface (Komor et al., 1988; Reimold et al., 2005). Whilst the subsequent Gravberg-1 project, launched in 1986, found no reserves of economic viability (Cole, 1996), the site remains an area for prospecting by the energy supplier AB Igrene, and strong concentrations of methane gas have been detected in drilling operations beneath the Ordovician and Silurian sediments (Drake et al., 2019).

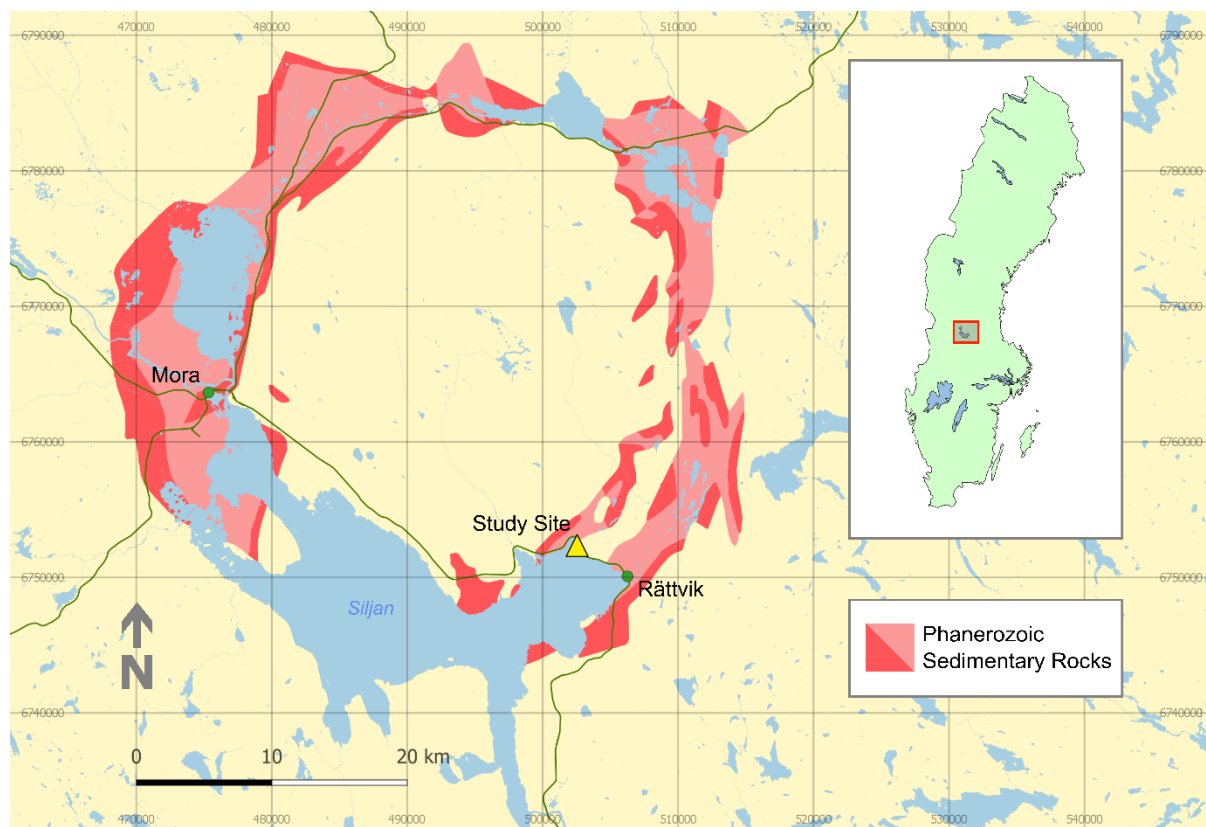


Figure 1.2. Map of the Siljan impact structure, highlighted by the ring of preserved Ordovician and Silurian sedimentary rocks. The location of the study site in the south-east of the ring is marked by a yellow triangle. CRS: SWEREF 99 TM, Source: Lantmäteriet and Sveriges Geologiska Undersökning.

Whilst subsurface formation of methane can be abiotic (through inorganic reaction of compounds such as H₂ and CO₂), it can also be formed thermogenically by organic matter breakdown, and through microbial activity, with the origin being determined by the $\delta^{13}\text{C}_{\text{CH}_4}$ isotopic signature. Abiotically generated methane in general exhibits less depleted values up to -35‰, thermogenic moderately so between -35‰ and -50‰, whilst microbially formed methane has a very light signature of -60‰ or lower (Whiticar, 1999; Drake et al., 2019). The methane gas detected in Siljan has been shown to have a $\delta^{13}\text{C}$ signature of around -64‰, implying a biogenic origin at odds to Gold's theory, though lower values of the ratio between methane and higher hydrocarbons implies there is a strong thermogenic influence as well (Drake et al., 2019). A biogenic origin is also supported by the evidence of microbial methanogenesis seen in secondary calcite precipitates in the area (Drake et al., 2019). Precipitation of heavily $\delta^{13}\text{C}$ depleted carbonates is used as a tracer for sulphate dependant anaerobic oxidation of methane in marine sediments, with less $\delta^{13}\text{C}$ depleted deposits attributed to cementation from dissolved inorganic carbon generated during microbial methanogenesis (Drake et al., 2015; Budai et al., 2002). Calcites with lighter $\delta^{13}\text{C}$ signatures sampled from fractures elsewhere around the Siljan area are therefore interpreted to be a by-product of anaerobic oxidation of methane, whilst calcites with heavier signatures are argued as being characteristic of microbial methanogenesis (Drake et al., 2019). Presence of precipitated calcite within the fractures of the study site could therefore be evidence of anaerobic oxidation of methane, which as part of a redox reaction would have resulted in the reduction of the iron oxide in the limestone. Calcite with heavier signatures could of course also be abiotic in nature, and there are instances where calcite precipitated from abiotic methane of hydrothermal origins display significantly depleted $\delta^{13}\text{C}$ values due to fractionation and reduction processes (McCollom et al., 2010). Using isotopic signatures to distinguish between abiotic and biotic methane origins can therefore be misleading, which makes establishing the origin of any methane which was involved in the creation of features seen at the study site potentially challenging (Kietäväinen & Purkamo, 2015).

1.4 Timing of hydrothermal events

Regardless of the source of any methane mobilised through the fractures at the study site, the timing of this mobility in relation to the impact is also unclear. If considering a hydrothermal system to be the cause of this mobility, two possible options present themselves from existing evidence:

Simultaneous with the impact

Long term hydrothermal systems, of which there is mineral evidence in the Siljan Ring, are an accompanying feature of impact craters due to the transfer of kinetic energy at the site and the interaction of meteorite debris with the local hydrosphere (Naumov, 2005). A hydrothermal system simultaneous with the impact is therefore a strong candidate for mobilising a methane bearing fluid within the fractures of the study site. Sulphide mineralisation within veins in similar limestone deposits in the area show a relation to local thrust and fault zones, directly connecting it to tectonic activity which accompanied the meteorite impact (Johannsson, 1984).

Post-impact

The low salinity and concentration of fluid inclusions found in quartz grains in granites and within contact veins elsewhere around the impact site, whilst hydrothermal in origin, exhibit cross-cutting relations indicating that some post-date the impact (Komor et al., 1988). A lack of fluid inclusions within some of the secondary calcite precipitates implies a low temperature origin possibly unrelated to the impact, which is supported by U-Pb dating which indicated these minerals to having been formed between 80 and 20 Ma (Drake et al., 2019).

Where the fluid which was active at the study site fits within this timeline remains to be seen. A hydrothermal event prior to the impact theoretically remains an option, though any evidence for this would be dependent on when the fractures found at the study site were formed.

Aim

The aim of this study is to determine the reaction whereby the haloes are formed, and thereby attempt to constrain the timing of fluid mobility along fractures at the study site based on structural, petrological, and geochemical data obtained in the field and in thin section. If these fractures are methane-bearing, the results of this study can help to constrain the origin and timing of methane production and mobility in the Siljan Ring.

2. Methodology

Data for use in the study was obtained primarily through three methods: structural analysis of bed, joint, and fracture orientation across the field site; XRF analysis across individual haloes and the surrounding country rock; and analysis of thin sections made from a sample of a halo and surrounding country rock.

2.1 Structural Analysis

Fracture orientation in relation to bedding, joints, and regional structures is key in establishing the relative timing of their formation and determining which events fluid mobility and halo formation post-date. Continuation of these trends within microstructures observed in thin section can also support any conclusions.

A structural investigation of the site was conducted in October 2023 to establish the strike of the haloed fractures, as well as the orientation and dip of the limestone bedrock. These measurements were recorded using the Lambert clinometer application on an iPhone SE, which plotted dip, dip direction, and strike, as well as the GPS coordinates of the bed or fracture in question. The application proved reliable, though was occasionally sensitive to the magnetic field produced by other field equipment. As such, the gyroscope was regularly recalibrated, with a hand-held compass and spirit level being used to confirm its orientation prior to measurements being taken again. These data were then uploaded into QGIS and a map constructed to relate fracture and halo orientation to the limestone beds and the wider geologic structure of the Siljan Ring.

The latter part of the fieldwork was conducted after a period of extremely heavy rainfall in the region, and water levels in Lake Siljan were subsequently at a level which meant the majority of the study site and haloes observed in 2022 were submerged. As such, structural measurements were only possible at the highest point of the shoreline and were not able to be accurately conducted for the haloes which had been previously sampled as part of the XRF analysis. Any approximate orientations attributed to these haloes have been reconstructed using data obtained further along fractures towards the treeline and with the use of photographs obtained during separate visits to the field site.

Submersion of the study site also meant obtaining higher resolution imagery to use in constructing a more detailed map of the area was not possible, and existing remote sensing data obtained from Lantmäteriet was used instead.

2.2 XRF Analysis

X-ray fluorescence analysis involves the measurement of fluorescent emissions corresponding to a particular element produced by electron transitions within the innermost shells following irradiation of a solid sample. The weight percentages of various elements within that sample are then calculated, however the absorption of x-rays produced by elements with an atomic number lower than 9 means light elements are not individually measured and their composition is reported as a whole (Winter, 2014). Weight percentages can then be used to identify the rock, as well as plot any changes in composition over a sampled area.

XRF analysis of five haloes distributed across the study site was conducted a year prior in October 2022 using an Olympus Innov-X hand-held analyser. The approximate locations of these haloes are shown in Fig. 2.1 below. Fractures which crosscut over a broad extent of the surrounding beds were favoured in order to provide a representative sample, and analysis points were chosen based upon surface stability and areas where the haloes were most strongly visible, displaying the least amount of weathering. A tape measure was secured across the halo and samples taken at one-centimetre intervals, beginning and ending in the adjacent country rock. 140 samples were obtained overall which were then used to analyse various element weight percentages in the country rock, in the halo, and around the fracture and vein.

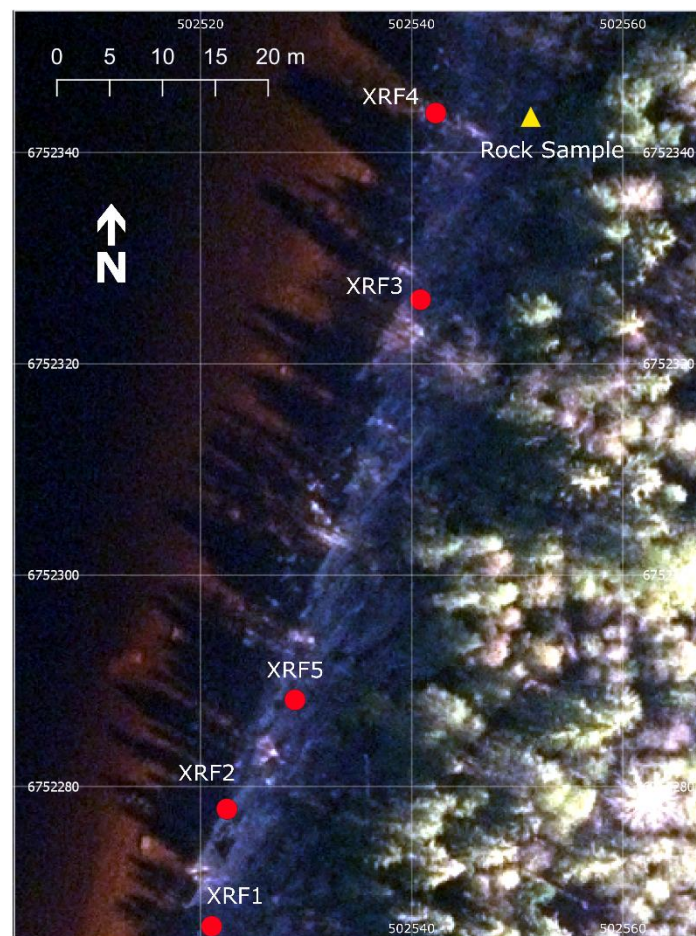


Figure 2.1. Satellite image of the study site showing XRF analysis locations and the point from which the rock sample used for thin sections was taken. CRS: SWEREF99 TM, Source: Lantmäteriet

2.3 Thin Section Analysis

Thin section analysis was conducted on a cross section sample of a halo in order to observe the mineralogy of the country rock, halo, and vein. Sample collection was undertaken in September 2023, which due to high water levels again meant selection was limited and the opportunity to sample from a halo analysed with XRF was not possible. An orientated sample across an entire halo and extending into the unaltered limestone was obtained from the northern most point of the study site shown in Fig. 2.1, with the rock cut into six pieces covering the country rock, halo, and vein, and then made into thin sections (Fig. 2.2). Mineral identification and textural analysis were done using a petrographic microscope. Due to a fault in the mechanical stage accessory, point counting was accomplished using high resolution images of the thin sections captured at 4000 dpi with a scanner. Using a graphics editor, a digital grid consisting of 8410 points was placed over an image and the mineral under each point was identified and recorded. Photographs captured with an adjusted exposure directly from the microscope were also used to conduct a raster image analysis in QGIS to establish certain mineral percentages more accurately at different points around the vein.



Figure 2.2. Rock sample from the study site (left), and the six pieces prepared for thin section with their orientation (right).

3. Results

3.1 Structural Analysis

Fig. 3.1 on the next page shows a map of the study site with measured orientations for the bedding, haloed fractures, and joints which were accessible at the time of field work. SGU's bergkartvisare reports dating for the limestone of around 455 to 443 Ma in the Katian and Hirnantian ages of the upper Ordovician (SGU, 2023). The limestone bedding dips towards 300° northwest at a dip angle of around 25° , corresponding to the depressed graben surrounding the central plateau of the Siljan impact structure within which Phanerozoic sediments have been preserved. The study site's location on the outer 'wall' of this graben is highlighted in Fig. 3.2. Dip direction and dip were not recorded for

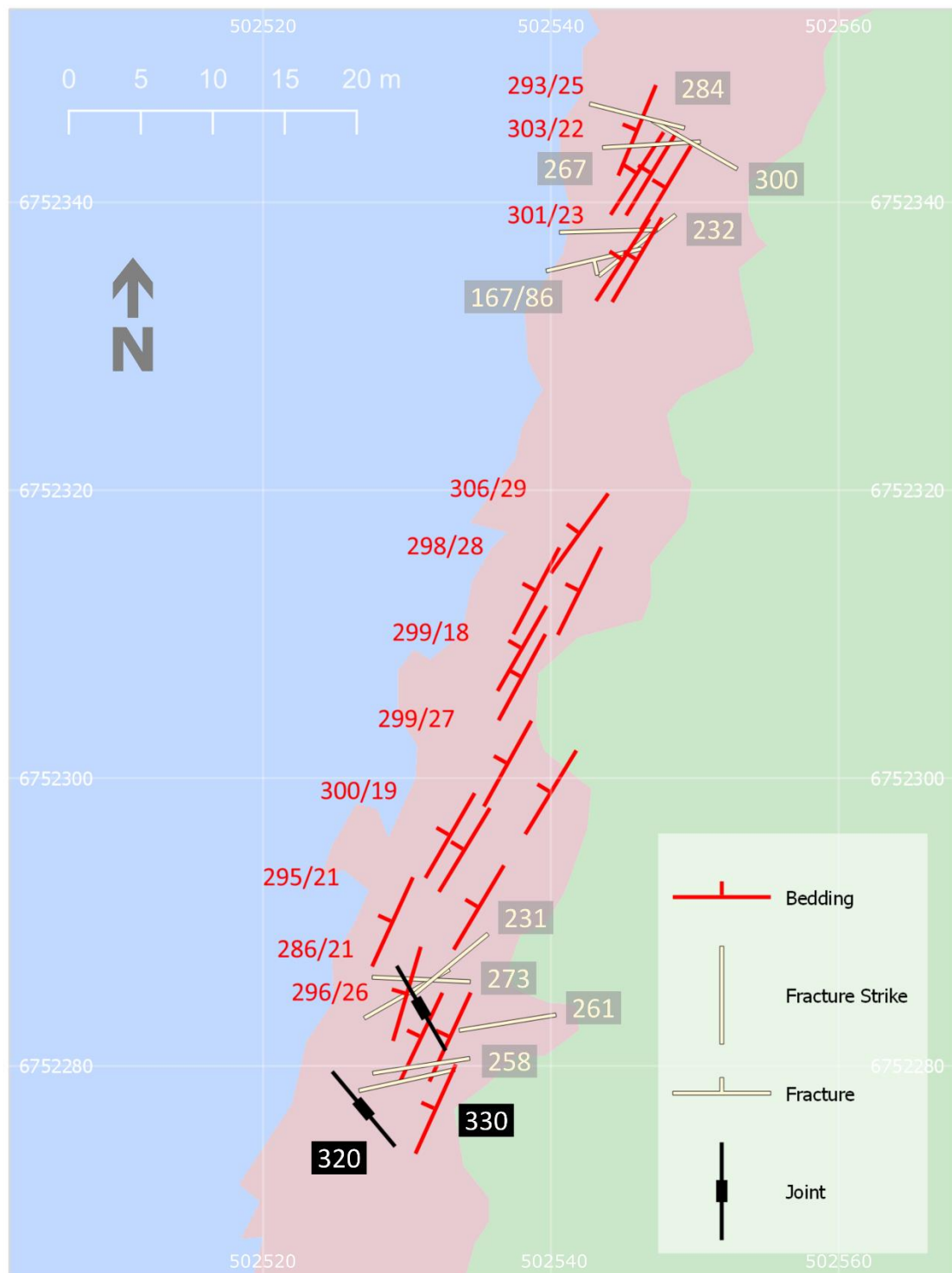


Figure 3.1. Map of the measured structures at the study site, showing bedding, fractures, and joints, alongside their strike or dip direction/dip. The limestone beds can be seen to have an average dip direction/dip of around 300/25. Larger haloed fractures are generally orientated east to west, with a strike azimuth of around 250-270°, though examples of fractures interconnecting to form grid-like patterns are shown in Fig. 3.3. The one fracture for which a dip was measured is shown to be near vertical. The two joints measured orientate more towards north. CR: SWEREF 99 TM, shoreline boundaries adapted from Lantmäteriet.

the haloed fractures as a fracture plane was only observable at one point across the site. Subsequently it is the strike azimuth of the fracture through the bedrock which is reported in Fig. 3.1, which shows most haloed fractures to have a strike of between 250° and 270° . For the one fracture where the plane was visible, dip angle was recorded as near vertical. The strike of most fractures corresponds to the strike of one of the major faults in the area, as seen in Fig. 3.2, which is part of a wider network of local concentric faults encircling the central plateau of the region. As seen in Fig. 3.3, there are instances where fractures interconnect on a smaller scale, forming grid-like patterns which lack crosscutting. As shown in Fig. 3.2, the study site along the major local fault all lies within a 65km wide zone of complex, intense fracturing directly related to the Siljan impact (Kenkmann & von Dalwigk, 2000).

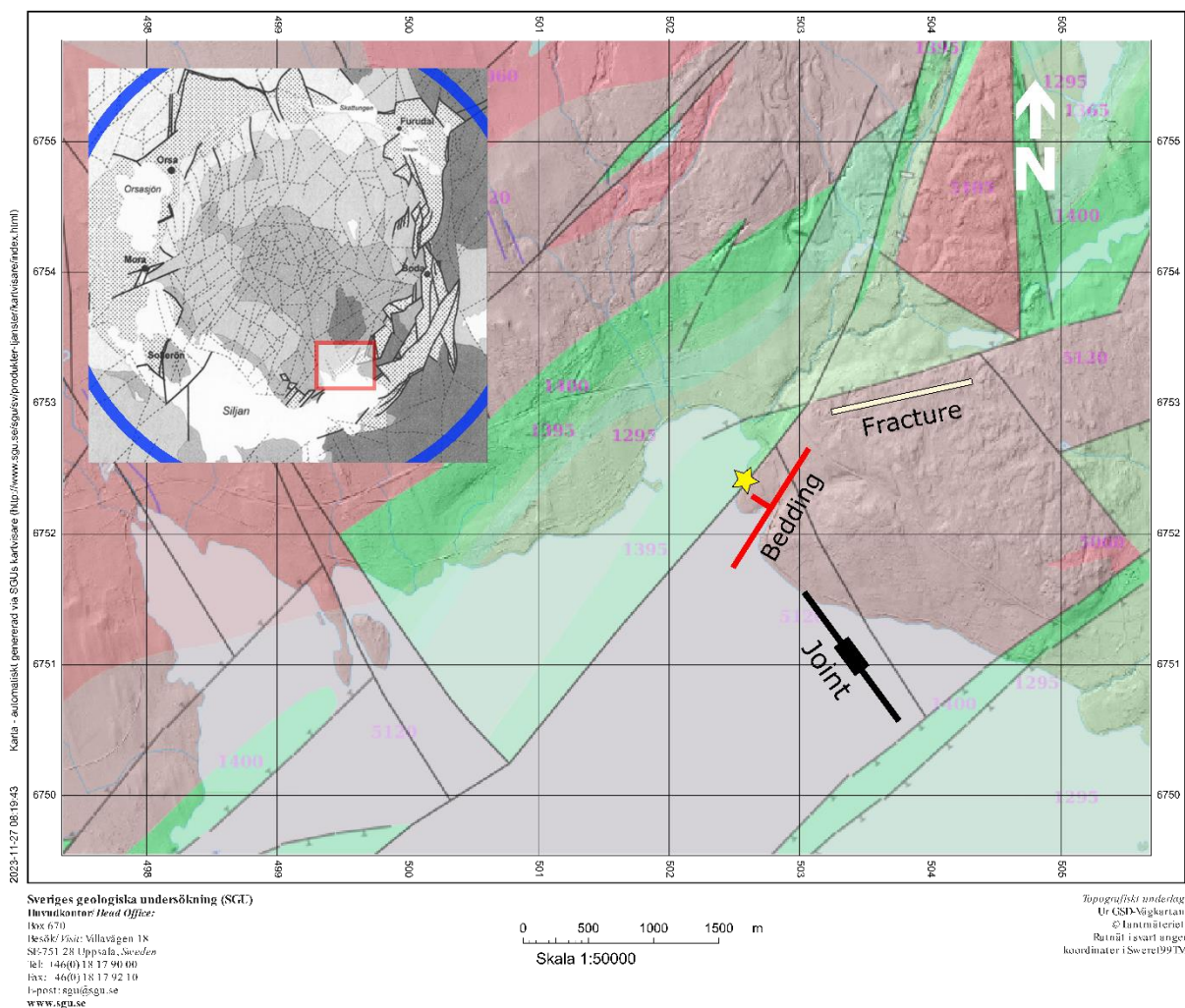


Figure 3.2. Map showing faults and deformation in the area beyond the study site (yellow star) and in the wider region. Inset map shows the impact crater and the fault system related to this which the study site (red box) lies on, along with a 65km wide zone (marked in blue) of complex, intense impact related fracturing identified by gradients in the fracture density and pattern (adapted from Kenkmann & von Dalwigk, 2000). Average bedding, joint, and fracture orientations from the study site are shown on the map of the wider area. The majority of haloed fractures align with a major concentric fault related to the impact structure. Bedding dips relative to another deformation forming the outer wall of a graben containing early Devonian sandstone at its centre. Joints are also roughly orientated to radial fault fractures emanating from the central plateau of the impact structure. Source: Sveriges geologiska undersökning and Lantmäteriet.



Figure 3.3. Two examples of where haloed fractures are seen to interconnect, forming grid-like patterns in the bedrock.

The reaction haloes themselves are seen to vary in width between fractures, as seen in Fig. 3.3 and Fig. 3.5, and their boundary with the country rock is also sharper and more intense in some places than in others, as seen between haloes 1 and 3 in Fig. 3.5. However, it is likely that subsequent weathering has as much a part to play in this as any fluid event which may have instigated a reaction. Haloes are also observed to extend evenly along the entire fracture, with no breaks or displacements, or points where the haloes narrow or becomes broader. Also noticeable, as shown by the measuring tape in Fig. 3.5, is the symmetry displayed by the haloes either side of the vein. These factors are important in characterising the uniformity of fluid flow within fractures at the site, and the implications this has for its origin.

Joints can also be seen at the site, both on the small and larger scale, though only two locations were able to be measured as part of the fieldwork. These might possibly be related to a larger fracture in the area, as highlighted in Fig. 3.2, though the limited data makes this difficult to verify. If correct, these joints may be connected to radial fractures related to the impact structure. Joints can be seen to crosscut the haloed fractures as shown in Fig. 3.4, which combined with their lack of reaction haloes suggests they post-date any potential fluid event, and by association the halo-bearing fractures, and may therefore be the result of a later stress and deformation event.

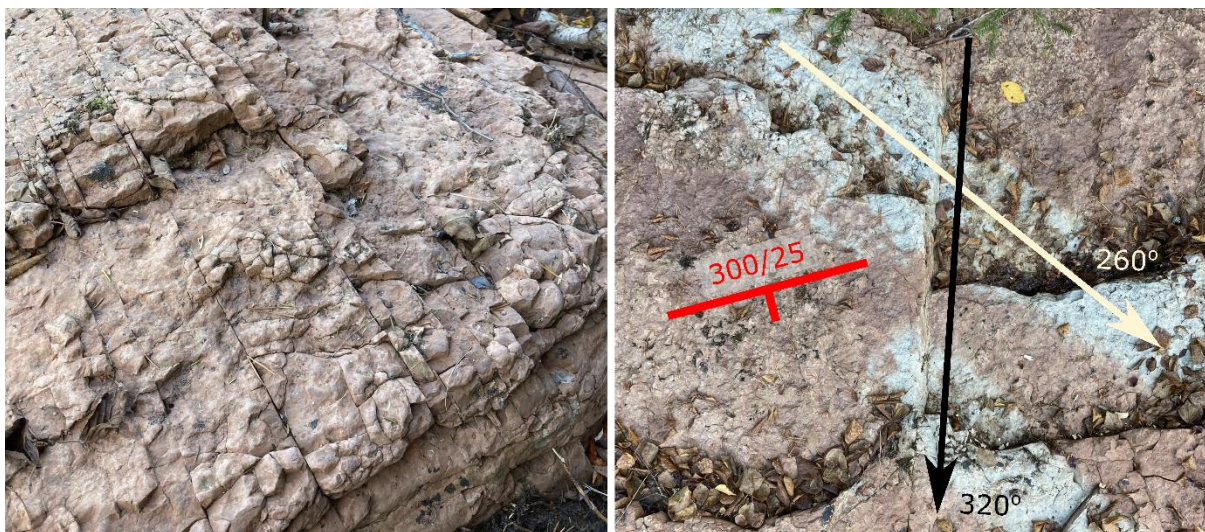


Figure 3.4. Example of joint systems seen at the site (left), and an annotated image showing a larger master joint (black line) crosscutting a haloed fracture in the limestone beds.

3.2 XRF Analysis

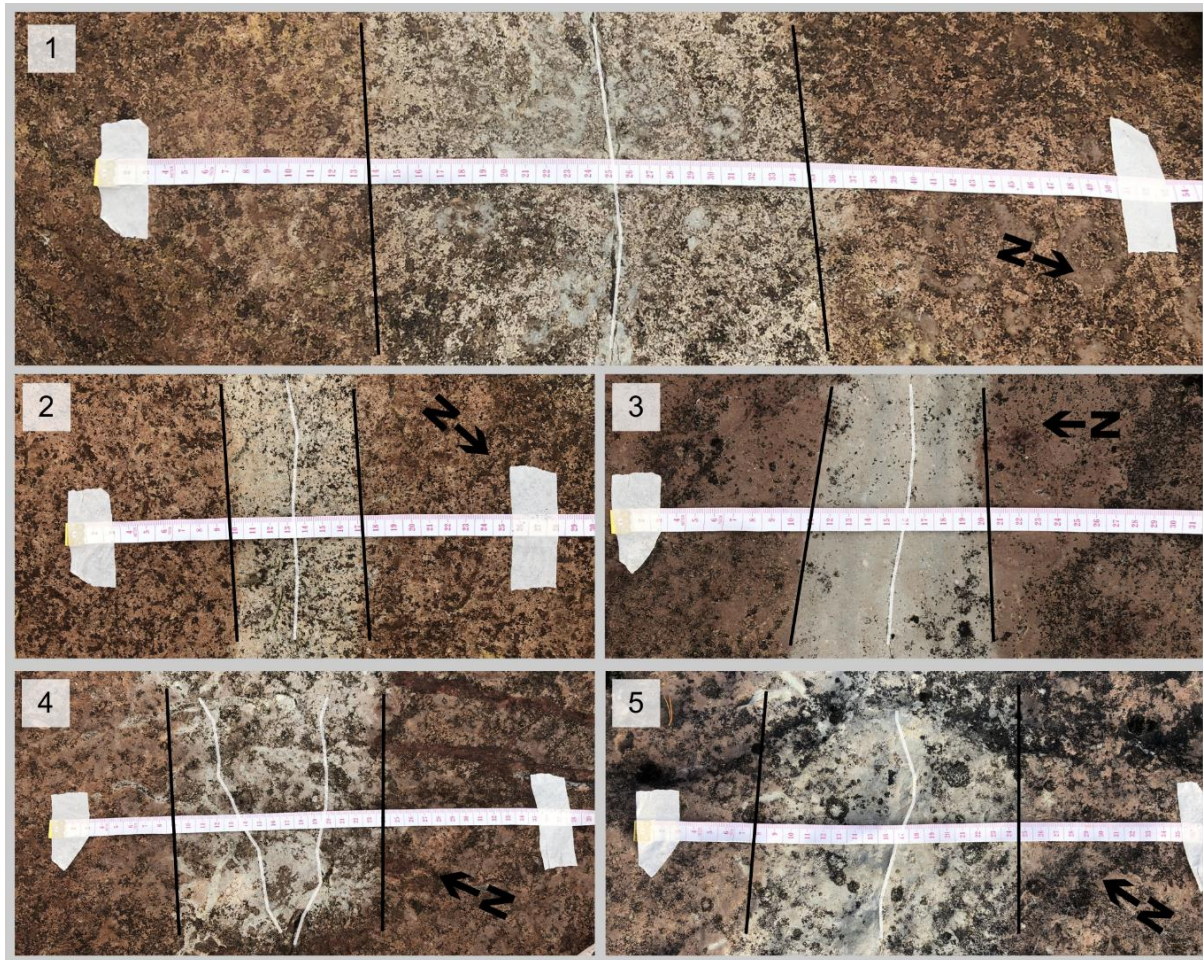


Figure 3.5. The 5 haloes sampled using the XRF analyser. Black lines indicate reaction area boundaries, vein locations are highlighted in white. Approximate orientation is indicated based upon relation to bedding and other photographs from the study site, though fracture strike is generally 250° to 270° . Using the tape measure for reference, whilst haloes can vary in size symmetry is nonetheless maintained.

Five haloes were sampled for XRF analysis as shown in Fig. 3.5 above, with the weight percentages of various constituent elements recorded. Data manipulation involving normalisation was not required in this instance as weight percentages already showed noticeable concentration variances, the most significant being in iron and sulphur values. Peaks or occurrence of other elements, mainly metals such as zinc, copper, and lead, were also observed at or around the vein consistently across all sample sites. Fig. 3.6 on the next page shows the weight percentages of iron and sulphur in the country rock, halo, and vein for the five sampled halo sites marked on the map in Fig. 2.1. Concentrations are shown to fluctuate between approximately 1-3% for iron, and 0.1-0.5% for sulphur. Relatively speaking, the country rock contains depleted amounts of sulphur and higher levels of iron. Moving into the halo reaction zone, iron concentrations drop before sometimes recovering slightly around the vein, whilst sulphur concentrations in contrast are seen to increase before peaking at or around the vein. Peaks of sulphur in haloes 3 and 5 are shown to be just left of the vein, which in both cases orientate northwards corresponding with bed dip direction, however it is possible (and more likely) that these peaks are actually located within the vein and have been mis-captured by the analysing equipment.

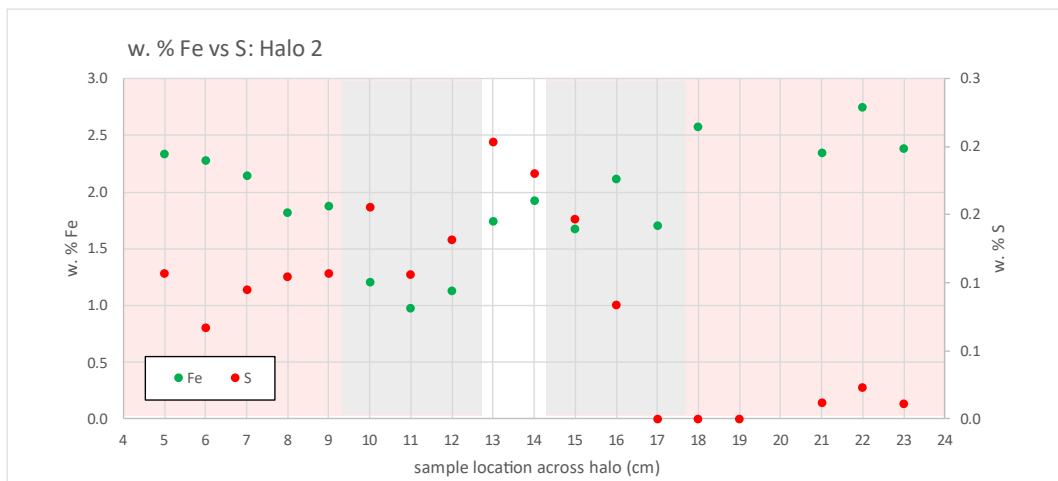
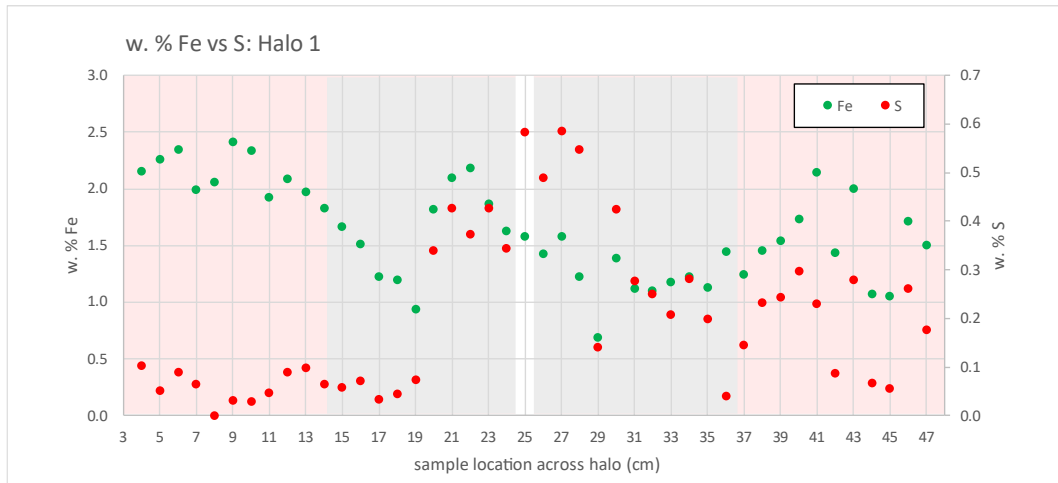


Figure 3.6 (continued on the next page). Reported weight percentages for iron and sulphur for sample haloes 1 to 5. Country rock is indicated by pink, the reaction halo by grey, and the vein by the white band. Iron levels can be seen to be relatively higher within the country rock, decreasing within the reaction halo towards the vein, before recovering somewhat in certain cases. Sulphur is relatively depleted in the country rock whilst displaying higher concentrations within the halo, peaking at or next to the vein.

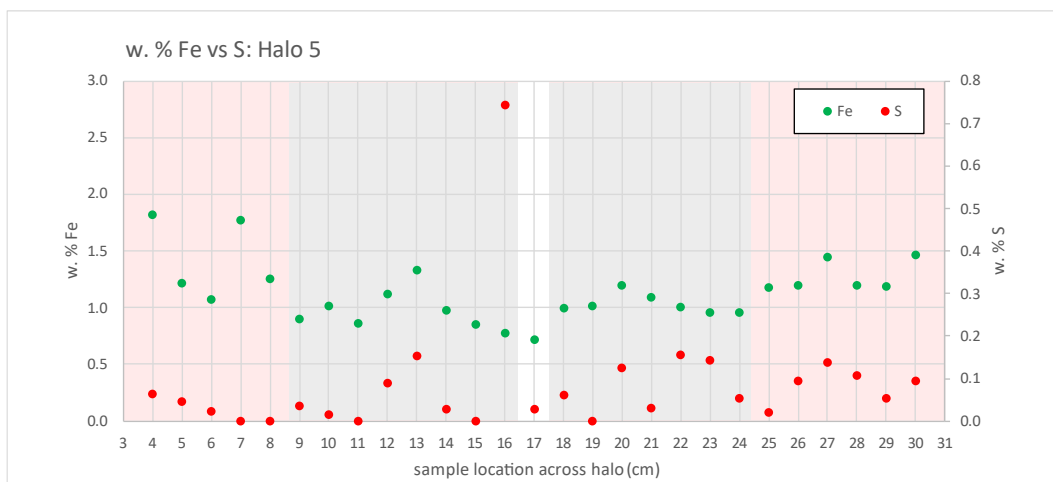
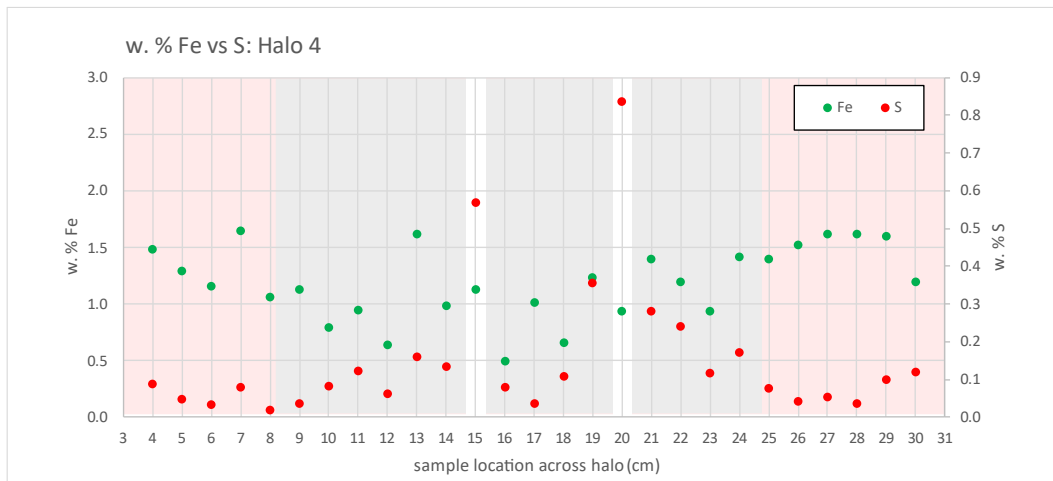
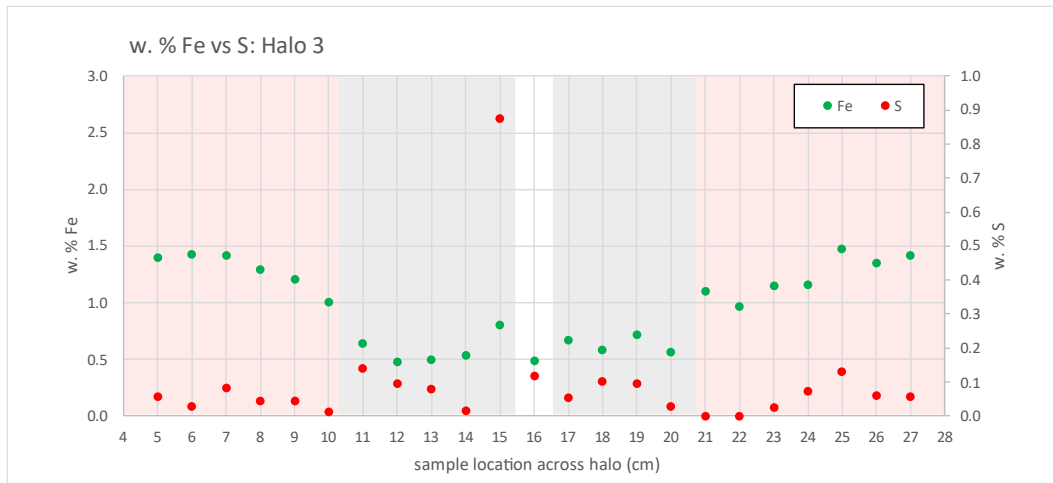


Figure 3.6 continued.

3.3 Thin Section Analysis

3.3.1 Microscopy

Thin sections 02, 04 and 05 are sampled from country rock to the south of the fracture. Fig. 3.7 consists of two images taken from thin section 02 which shows an allochem supported fossiliferous limestone consisting of siliceous fragments set within a matrix stained brown from iron oxides - the source of the distinct red colour of the limestone beds. The extremely small grain size of the matrix (better seen in Fig. 3.9) coupled with a high concentration of fossils suggests the limestone to be a packed biomicrite using the Folk and Dunham classification systems (Blatt et al., 2005).

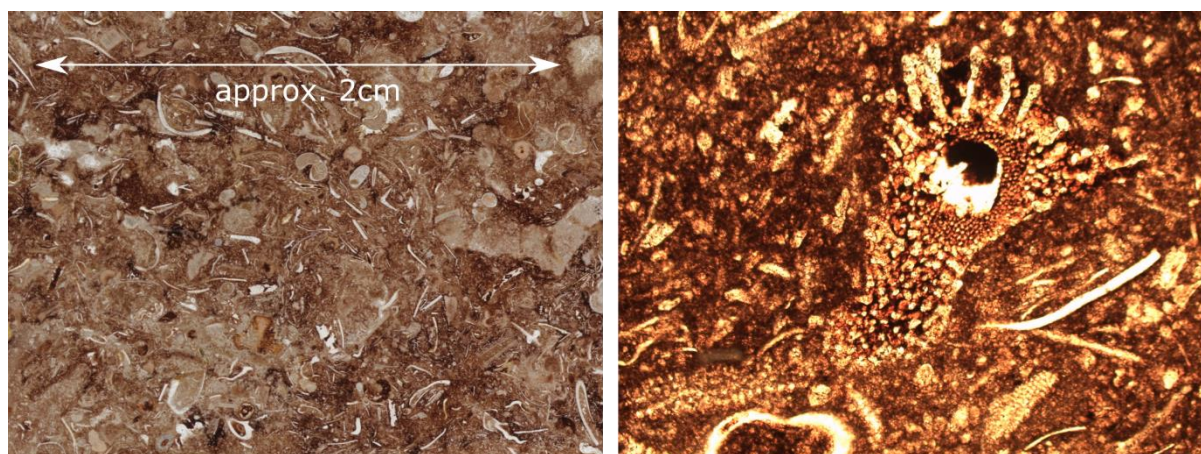


Figure 3.7. A high-resolution image of thin section 02 (left), and an example of the fossils within surrounded by a matrix stained with iron oxide (right, 10x objective PPL).

Whilst the matrix is dominated by iron oxides, inspection of the shells under cross polarized light show many to have recrystallised into minerals of either first or high order interference colours as seen in Fig. 3.8 to the right, likely quartz and calcite.

Allochems within these samples are well preserved – fossils maintain their original form and curvature, and there is little evidence of realignment or breakage which would be expected had the rock experienced significant heat or pressure related to metamorphism or an orogenic event.

Moving towards the vein a clear boundary can be seen marking the transition from the oxidised country rock into the reaction zone halo. Within the halo the composition is largely the same as the country rock, with a duller micritic matrix now revealed in the absence of the iron oxide. Fig. 3.9 shows this boundary in thin section 03, and the halo is more broadly captured in Fig. 3.10 from thin section 06.

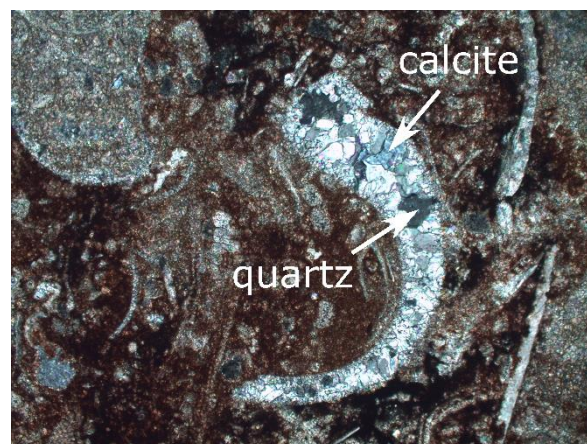


Figure 3.8. Recrystallised shell fragments as seen in thin section 04. 10x objective XPL.

Notably, the iron oxide on the edge of the reaction zone can be seen clustered around opaque minerals in Fig. 3.9, which is not otherwise observable in the country rock. These minerals are also seen scattered throughout the halo in Fig 3.10.

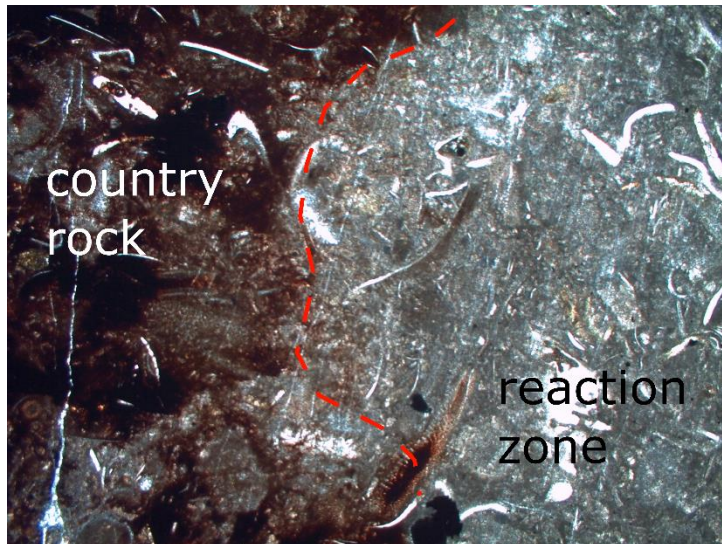


Figure 3.9. The transition in thin section 03 from the oxidised country rock on the left, to the reaction halo on the right where the matrix takes on the dull colour and fine texture of a micrite. In this example, iron oxide is more clearly seen to centre around opaque minerals on the edge of the reaction zone. 2.5x objective XPL.

The vein itself consists of much larger, colourless crystals with moderate relief when view in polarized light (Fig. 3.10). Under crossed polarities in Fig. 3.11, these minerals have high order interference colours and display distinct banding, characteristic of the deformation twinning seen in calcite or dolomite. Whilst the crystals are generally uniform in size, smaller fractures and secondary veins within the main vein can be seen containing much smaller calcite crystals or dark, opaque minerals.

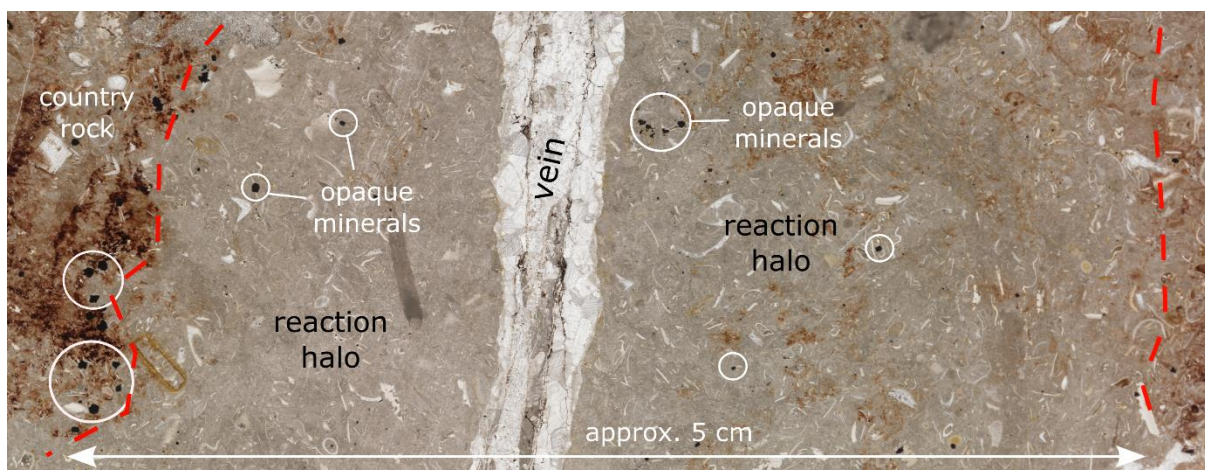


Figure 3.10. A high-resolution image of thin section 06 showing the oxidised border of the country rock at its edges, the vein consisting of a colourless mineral running through the centre, and the reaction halo either side where opaque minerals are scattered through the dull grey biomicrite.

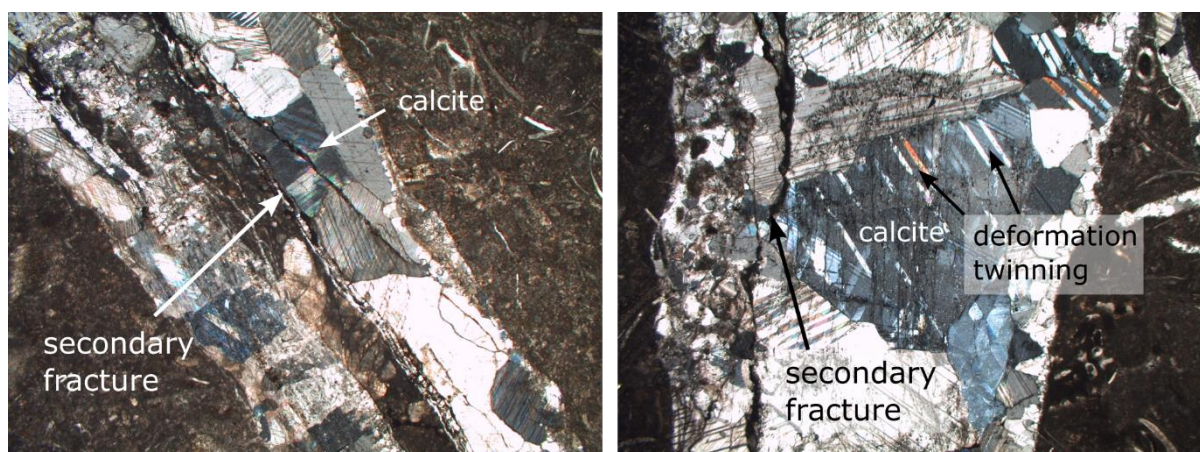


Figure 3.11. The vein viewed under cross-polarized light in thin section 06 (left, 10x objective), and in thin section 03 (right, 20x objective). Various sized calcite crystals with high order interference colours and deformation twinning have precipitated within the fracture, as well as within smaller fractures running parallel within the vein and along its edge.

Also seen in Fig. 3.9, and highlighted in more detail in Fig. 3.12 below, are parallel microfractures seen cutting across the structure of the rock. It is somewhat difficult to tell whether these microfractures are an extension of the fracture within which the vein has precipitated, given that they are observed as containing a similar precipitation of calcite, or whether they are stress fractures connected to the joint system seen elsewhere at the field site as highlighted by their orientation in Fig. 3.12. The joints seen in Fig. 3.4 were observed as lacking evidence of fluid interaction, so the presence of precipitated calcite within these microfractures implies they are more likely to be connected to the fracture and subsequent fluid event which formed the vein. Importantly, as seen in the two images on the right in Fig. 3.12, these microfractures clearly crosscut the opaque minerals, proving these minerals to be part of the original composition of the limestone and not something which has subsequently formed in the reaction halo as a result of hydrothermal activity in the vein.

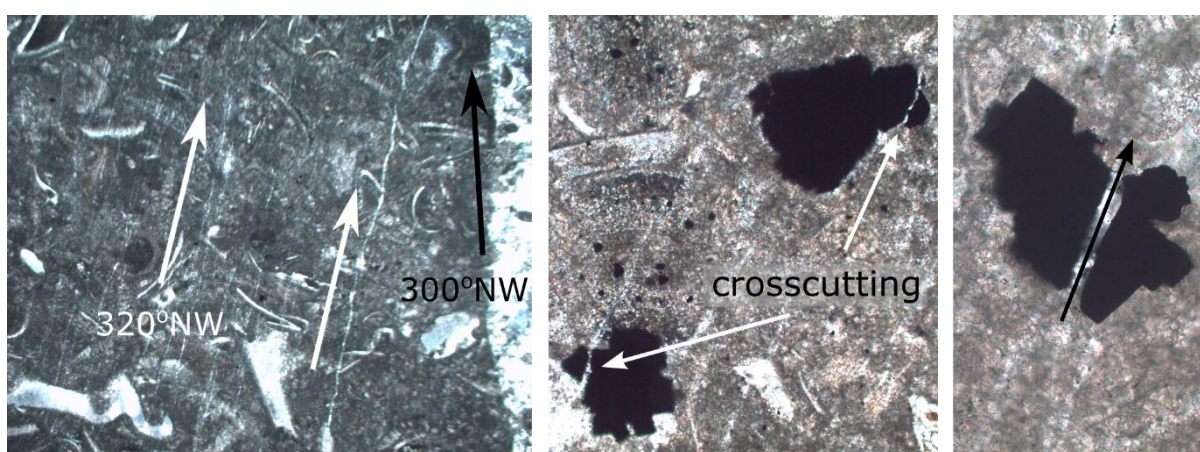


Figure 3.12. Microfractures (left, 2.5x objective XPL) as seen in thin section 03, with orientation highlighted in white and compared with that of the main vein (black). Evidence of microfractures crosscutting the opaque minerals (right, 20x and 40x objective XPL).

Further investigation of the opaque minerals using the reflected light source reveals them to be pyrite crystals - an iron sulfide with formula FeS_2 . They are only observable within the reaction haloes and occurrence in the country rock is extremely rare. The crystals are cubic in form, and under oblique reflected light display a bold, brassy yellow colour. The specimen in Fig. 3.13 is located towards where the halo meets the country rock in Fig. 3.10, and when viewed under reflected light and with varying exposures is revealed to be corroding away along its edges. The image captured with increased magnification in the bottom right of Fig. 3.13 shows existing cavities in the limestone filled with iron oxides or hydroxides emanating from the where the pyrite is reacting and corroding. In its place, calcite can be seen precipitating along the crystal edges which have reacted to produce the iron minerals. This provides an explanation for the iron oxide or hydroxides staining the rock around this specimen, as seen in the top left image captured with cross polarized light.

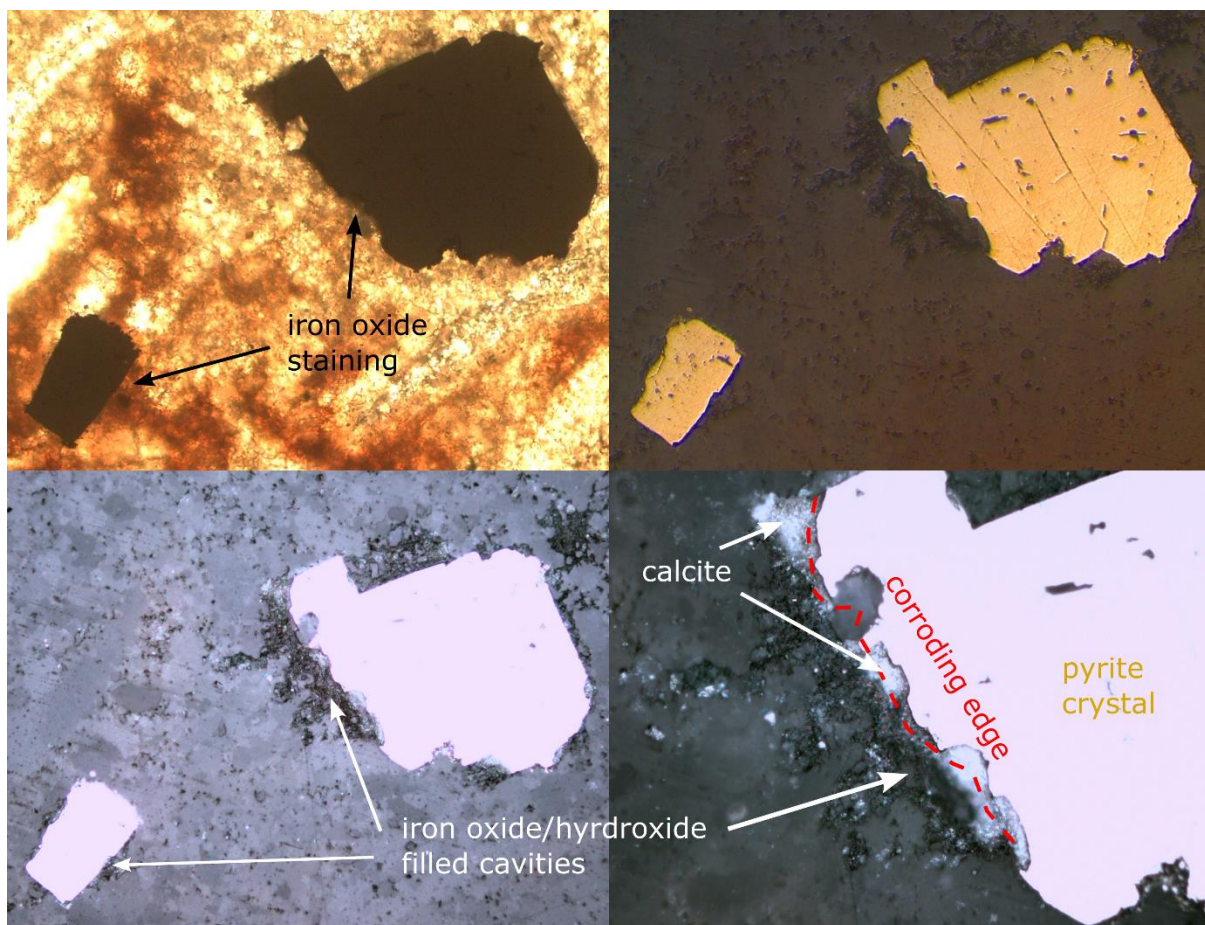


Figure 3.13. A pyrite crystal located at the halo boundary in thin section 06. The top left image shows the opaque crystal under cross polarized light with a 20x objective. The top right image is the same crystal under oblique reflected light. The bottom two images show the crystal under greater exposure, where evidence of corrosion can be seen along the crystal edges using the 40x objective in the bottom right image. Iron oxides or hydroxides can be seen emanating from the pyrite crystal, filling cracks in the limestone, with calcite precipitating in places where the pyrite has reacted away.

3.3.2 Point Counting

Point counting was conducted on a high-resolution image of thin section 01 taken under cross polarised light to allow for better mineral identification. Using the 8410-point grid, consisting of 146 x 59 cells, an area roughly 30 x 13 mm centred over the vein was covered with each cell representing an area of around 0.2mm². The point counting results are shown in Table 1 below, which shows the mode and equivalent volume percentage for each mineral as well as the error margin required for 95% confidence in the results. The same exercise was also conducted on a similarly size area of thin section 04, which is sampled from country rock furthest outside the reaction zone. Oxidation intensity was ignored, though almost all siliceous fragments can be seen to be stained with some degree of iron oxide.

Thin Section 01					Thin Section 04				
	Siliceous Fragments	Calcite	Pyrite	Opaque Vein		Siliceous Fragments	Calcite	Pyrite	Opaque Vein
Points	7254	1099	40	17	Points	8116	291	3	n/a
%	86.25%	13.07%	0.48%	0.20%	%	96.50%	3.46%	0.04%	n/a
+/-	0.75%	0.74%	0.15%	0.10%	+/-	0.40%	0.40%	0.04%	n/a

Table 1. Point counting results showing the volume percentage of minerals in thin section 01 and thin section 04. Reliability margins are provided based on van der Plas & Tobi (1965).

Calcite volume is higher in thin section 01 as it also includes the vein, whereas in thin section 04 it is only seen recrystallised within shell fragments. However, the results clearly show that pyrite is present in the reaction halo around the vein whilst almost non-existent in the country rock. It is not impossible that some pyrite crystals, which appear opaque under cross polarized light, are obscured by more intense patches of iron oxide. However, as seen in Fig. 3.13 pyrite decomposition is shown to be a source of oxides within the rock and it is therefore unlikely that intact pyrite crystals would remain under darker patches of iron oxides.

Point counting shows pyrite to be the key variance in mineralogy between the country rock and reaction halo, though more localised volume percentages may help to highlight any local trends and show more accurately how the pyrite is distributed throughout the rock.

3.3.3 Image Analysis

Due to the unique optical properties of opaque minerals making them particularly striking under reflected light, a calculation based on pixel colour levels from a high-resolution image can provide an even more accurate percentage of pyrite volume than can be achieved through point counting.

Images were captured using a 5mm wide field of view at intervals to the left and right of the vein at the top, middle, and bottom of thin sections 01 and 06. The photographs were taken under reflected light with an adjusted exposure with brightness levels 50%, gamma to 1.6, and saturation to 100%. This produced images such as that on the left in Fig. 3.14, where pyrite crystals appear bright white, and the siliceous matrix is extremely dark. These images were then uploaded into QGIS where a raster calculation was performed to isolate all pixels with RGB values in bands 1, 2, and 3 of 100 or greater by returning a value of "1" (i.e. all pixels comprising pyrite crystals), and "0" for everything else.

The output of this raster analysis is shown on the right in Fig. 3.14 below. The images were then split into five 1mm wide areas and the percentage of pixels with a value of 1 within each area was recorded. The results of this count from thin sections 01 and 06 are shown in Fig. 3.15.

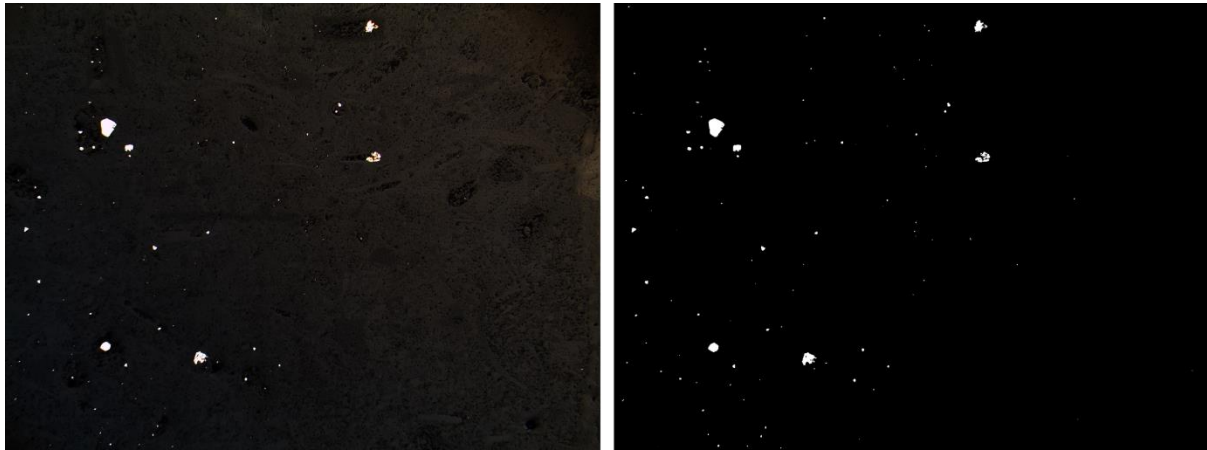


Figure 3.14. The image on the left shows pyrite crystals in the 5mm to the left of the vein in thin section 01 captured with reflected light and with adjusted exposure. The image to the right is a raster image produced using QGIS which has assigned all cells identified as pyrite a value of 1 (in white), and everything else a value of 0 (black).

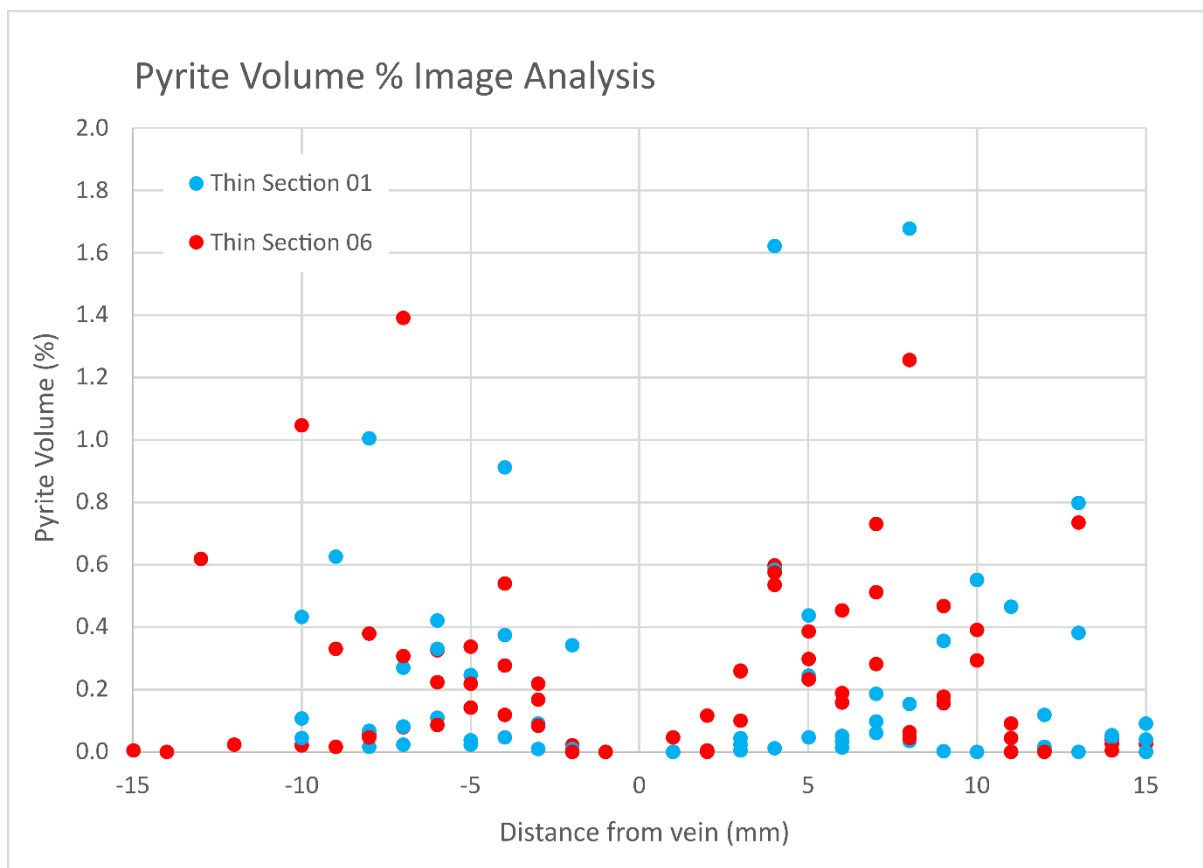


Figure 3.15. Pyrite volume percentages for thin sections 01 and 06 obtained from raster image analysis. The three results for each thin section at each distance represent values from the top, middle and bottom of the slide. Pyrite is observed as almost completely absent directly either side of the vein before increasing in occurrence within the reaction zone, with volume percentages decreasing again as the border with the country rock is approached.

Compared with the point counting exercise, pyrite compositions shown in Fig. 3.15 are broadly similar to the 0.48% reported for thin section 01. Image analysis however reveals that within millimetre wide areas pyrite is consistently absent from the 1-2 mm either side of the vein, before appearing in much greater quantities beyond this. This can also be observed in Fig. 3.14, where the far right of the images corresponds to the vein border and the adjacent rock is seen lacking in pyrite. Pyrite quantities are shown to increase from 3mm either side of the vein to around 10mm, before reducing as the reaction halo approaches the oxidised country rock. Spikes in volume relate to sections containing particularly large crystals. As a comparison, the same exercise was conducted for a 25mm wide area in the centre of thin section 02, sampled from the country rock. For the entire area, an average pyrite composition of 0.00097% was recorded.

Image analysis is therefore able to support the initial pyrite results obtained from point counting, but also provide greater detail around how pyrite is distributed within the reaction halo and around the vein. This is important in establishing not only which reaction has occurred in order to form the haloes seen at the study site, but also the period over which the reaction event occurred if the mineralogy within the haloes is inconsistent.

4. Discussion

4.1 The halo-forming reaction

The reaction whereby the haloes were formed is strongly implied by the results of the field study to be related to varying iron and sulphur levels between the country rock and within the haloes, and by association pyrite occurrence and concentration between these two zones. Halo formation due to interaction with a fluid flow was initially hypothesised as having two possible causes, which coupled with pyrite occurrence presents two options:

1. A reduction reaction within the halo has altered the original mineralogy leading to the formation of pyrite.
2. A reduction reaction within the halo has preserved the original mineralogy, of which pyrite was an existing part.

A possible redox reaction which saw iron being removed within the haloes would certainly be supported by the reduced iron concentrations in the reaction zone seen in the XRF data. However, the reaction textures seen in Fig. 3.13, which shows pyrite crystals corroding along their edges and producing the iron oxides/hydroxides which have stained the country rock, is evidence that they are part of the original mineralogy of the limestone, and not something formed afterwards. The second option of a reaction within the halo preserving the original mineralogy is therefore the one most strongly supported by the data in this study.

Pyrite is a widespread sedimentary mineral formed during early diagenesis from detrital iron and hydrogen sulphides and plays an important role in controlling sulphate levels in the ocean (Berner, 1983). It is therefore not unusual that pyrite should form part of the original mineralogy of the limestone beds. In addition to the reaction textures seen, crosscutting of pyrite crystals by subsequent microfractures is further evidence that these are original features of the rock, and not something which has crystallised afterwards within a reaction zone. Pyrite breakdown is subsequently the likely source of the iron oxides/hydroxides seen within the country rock, being a final product of pyrite oxidation (Hu et al., 2006), and this is evidenced by point counting and image analysis which shows pyrite to all but disappear from the mineralogy of the limestone beyond the halo.

This interpretation of the microscopy analysis is supported by the XRF data for haloes 1 to 5 which shows that within the halo area iron is depleted whilst sulphur is more abundant when comparing both to the oxidised country rock. The apparent decrease in iron can be explained by the fact that within the halo iron is held in more sparsely distributed pyrite (FeS_2), whereas in the country rock the breakdown of pyrite has resulted in iron oxides being transported throughout the entire matrix of the rock. The varying sulphur levels between the halo and country rock respectively correspond to the presence or absence of pyrite.

If the reaction zone therefore represents a 'preservation' rather than an 'alteration' halo, similar to that studied by Kleine et al. (2014), it means the original composition of the limestone has remained unaltered during an oxidation event which has given the country rock its distinct red colour. Two further important conclusions can be drawn from this:

1. That in order to preserve the original mineralogy of the limestone in the halo, a reducing agent has been present within the fractures which has counteracted the effects of oxidation.
2. This reduction event must have happened simultaneously with the oxidation event for this effect to occur.

4.2 Fluid chemistry

The evidence of a powerful reducing agent is a strong argument that methane detected elsewhere in the Siljan area, whether within a natural reservoir or involved in the formation of secondary precipitates, has likely also been active at the study site at some stage. Evidence exists in alternative environments of pyrite preservation sharing a positive correlation with methane flux (Lan-Feng et al., 2018), and it is reasonable to conclude that is what is being witnessed at the study site as well.

That this methane may be biogenic in origin is supported by the secondary calcite seen precipitated within the vein in thin section, which could indeed be another example of methane derived calcite deposits observed elsewhere in the Siljan Ring (Drake et al., 2019). However, this could just as well be calcite that has recrystallised from dissolved calcium carbonate carried by fluids within the fracture. As previously discussed, whilst using $\delta^{13}\text{C}$ isotopic signatures does not provide definitive proof of whether a methane derived secondary carbonate is of biotic or abiotic origin, in this instance it could be useful in establishing whether the isotopic signature of the calcite in the vein is at least different from that of the limestone. A different signature could signify influence by a different source, such as an abiotic methane reservoir or microbial activity, depending on $\delta^{13}\text{C}$ depletion. Presence of precipitated calcite is therefore not proof in itself of methane activity at the study site, however the fact a reducing agent has been involved strongly suggests a methane bearing fluid being responsible for forming the reaction haloes.

Evidence that this fluid likely has a hydrothermal origin is seen in the spike in metals recorded in the vein, as hydrothermal systems are often linked to ore deposits of minerals such as zinc, copper, and lead transported by fluids circulating through the earth's crust (Winter, 2014). The uniformity of the reaction haloes across the site in fractures with near vertical planar orientation (at least in one measurable case) also indicates a single, intense, hydrothermal event rather than a series of low-pressure flows which would have concentrated fluid differently within the fractures and produced asymmetry and varied width in the haloes.

4.3 Timing of the hydrothermal event

Establishing the timing of this hydrothermal fluid in relation to the Siljan impact can be achieved by framing these conclusions regarding the preservation event in the context of the structural evidence and data collected at the study site.

The age of the limestone bedrock of around 455 to 443 Ma means that the only significant tectonic event prior to the Siljan impact which might be responsible for the fracturing and downfaulting seen is the Scandian phase of the Caledonian orogeny, which current estimates argue to have begun around 430 Ma (Corfu et al., 2015). Evidence exists of this tectonic event having had an influence on the region, with an unconformity lasting from the middle Ordovician to the upper Silurian found in core samples taken from the western part of the ring, which has subsequently been attributed to erosion caused by tectonic loading of thrust sheets resulting from the collision between Baltica and Laurentia which began this process (Lehnert et al., 2013). However, this missing section of the stratigraphy is present in the eastern part of the ring just north of Rättvik (Lehnert et al., 2013), meaning not all of the area was necessarily affected by these events to the same degree. The location of the study site in the south-east of the ring suggests it might have been similarly unaffected by orogenic events, which the lack of ductile deformation and grain alignment observed in thin section supports.

Whilst the Caledonian orogeny cannot be ruled out as the tectonic catalyst which created the structures seen at the study site, fracture and bedding orientation provides stronger evidence of the Siljan impact being a more likely candidate. The force of an impact responsible for a fault and fracture network of the scale seen around Siljan is also the most likely source of an intense hydrothermal event capable of simultaneously oxidising the pyrite in the limestone whilst preserving it around the fractures through the mobilisation of methane released from the earth's crust.

The consistent dip of the limestone beds into and towards a downfaulted area circling the central plateau shows the study site to lie right on the edge of the impact's centre, and well within the zone where impact related features such as intense fracturing would be expected (Kenkmann & von Dalwigk, 2000). As seen in Fig. 3.2, the majority of haloed fractures also record a strike which matches the orientation of a nearby fault seen to form part of a system of others encircling the central plateau. Studies of the Siljan crater have shown a gravitational collapse of the crater rim to involve a complex interaction of interconnected concentric and radial faults, even on the centimetre to metre scale, forming a pattern dominated by fixed sub-vertical fractures (von Dalwigk, 2004). The near-vertical dip of the haloed fractures and their concentric orientation relative to the impact centre implies them to be part of this impact fracture pattern. The instances of fractures interconnecting even on a small scale, as seen in Fig. 3.3, also mirrors the description of concentric/radial fault interaction outlined by von Dalwigk (2004). Fractures which orientate slightly differently may be due to the complexity of this network, but also due to the fact the bedrock of the area today was originally 500 to 2000m below the earth's surface (with subsequent erosion removing the overlying layers) and may even have been transported 6 to 7km within the crater as a result of impact induced slumping (Ebbestad & Högström, 2007; Kenkmann & von Dalwigk, 2000).

Where the joints which are seen at the study site fall into these events remains harder to understand. Their orientation implies them to perhaps be a radial feature of the impact structure, however their cross-cutting relation to the haloed fractures suggests them to have formed later. As noted, the area has experienced significant movement and erosion since the time of the Siljan impact, and subsequent stress from events such as deglaciation could have formed additional joint networks. Similarly, whilst it was concluded that the microfractures seen in thin section are likely extensions of the concentric fractures linked to the vein (which is also supported by the fact this microfracture

pattern is lacking from the country rock in slides 2, 4, and 5), it cannot be ruled out that they may be related to the joint network instead. Observing microfractures in a sample where the vein is less orientated with the joint network and more towards the concentric fractures at 250° would perhaps be able to clarify which of the two the microfractures most align with, if indeed either of them.

4.4 Other hydrothermal events

Whilst the reaction which formed the haloes is the result of a single hydrothermal event linked to the impact, smaller fractures within the calcite veins containing finer calcite crystals and opaque minerals indicate subsequent hydrothermal events may have taken place, though perhaps not on the same scale as that generated by the Siljan impact. These events could have reactivated the fractures resulting in the multiple stages of infilling. This might also explain the absence of pyrite crystals in the 1-2mm surrounding the main vein, where more localised oxidising conditions could have led to their breakdown. It is possible that these smaller calcite veins are also the result of subsequent methane mobilisations and have an age similar to that of other younger precipitates found in the area, which dating using the same U-Pb method could confirm or refute (Drake et al., 2019).

4.5 Future work

It should be acknowledged that data collection in regards to structural evidence was not as extensive as initially planned, and conclusions drawn from this evidence are only based on a limited number of fractures and measurements. Interpretation is therefore based on what is considered reasonable given the available results. A more comprehensive map of fracture orientation and interconnectivity would help strengthen the interpretation of structural features at the site, and an opportunity to better explore the joint system and microfractures would perhaps help in understanding where they fit into events. Comparing the features seen at the study site with those found in other sedimentary rocks within the ring would also help in proving them part of a wider fracture network, though exposed Palaeozoic bedrock is rare within the area with most of the landscape buried beneath moraine and esker sediments deposited during deglaciation following the last ice age. The U-Pb dating method used by Drake et al. (2019) could also potentially confirm whether the interpretation of a hydrothermal event simultaneous with the Siljan impact is correct based upon the age of the calcite precipitates found within the haloed fractures.

5. Conclusion

Based on the petrological, geochemical, and structural data obtained in the field study, the reaction haloes surrounding fractures seen at the study site are shown to be formed by a reduction reaction involving a methane-bearing hydrothermal fluid. This fluid preserved the original mineralogy of the bedrock surrounding the fractures whilst the country rock beyond was simultaneously oxidised leading to the breakdown of existing pyrite in the limestone and the production of iron oxides. Structural analysis of the study site concludes this hydrothermal event and methane mobilisation to have been simultaneous with the Siljan meteor impact, with the fractures themselves forming part of a complex network of impact related features. Whilst methane from both abiotic and biogenic sources has been detected within the wider impact area, the source of the methane active at the study site remains unknown. Further investigation to establish the $\delta^{13}\text{C}$ signatures and U-Pb ages of calcite precipitated within the fractures may reveal this, and also confirm the timing of the hydrothermal event which formed the reaction haloes.

Acknowledgements

I would like to thank Alasdair Skelton for his valued support and feedback throughout my thesis project, and all the staff within the Department of Geological Sciences and the Department of Physical Geography who have guided me during my studies, especially during our excellent field trips. My thanks especially to my fellow distance students for their friendship and support over the last couple of years.

References

- Alizadeh, R., Jamshidi, E., Zhang, G. 2009. Transformation of methane to synthesis gas over metal oxides without using catalyst. *Journal of Natural Gas Chemistry*, 18, 124-130.
- Bar-Or, I., Elvert, M., Eckert, W., Kushmaro, A., Vigderovich, H., Zhu, Q., Ben-Dov, E., Sivan, O. 2017. Iron-coupled anaerobic oxidation of methane performed by a mixed bacterial-archaeal community based on poorly reactive minerals. *Environmental Science & Technology*, 51, 12293-12301.
- Beal, E.J., House, C.H., Orphan, V.J. 2009. Manganese- and iron-dependent marine methane oxidation. *Science*, 325, 184-187.
- Berner, R.A. 1983. Sedimentary pyrite formation: An update. *Geochimica et Cosmochimica Acta*, 48(4), 605-615.
- Blatt, H., Tracy, R., Owens, B. 2005. *Petrology: Igneous, Sedimentary and Metamorphic* (3rd edition). Freeman and Co., New York.
- Budai, J.M., Martini, A.M., Walter, L.M., Ku, T.C.W. 2002. Fracture-fill calcite as a record of microbial methanogenesis and fluid migration: a case study from the Devonian Antrim Shale, Michigan Basin. *Geofluids*, 2, 163-183.
- Cole, S.A. 1996. Which came first, the fossil or the fuel? *Social Studies of Science*, 26(4), 733–766.
- Corfu, F., Andersen, T., Gasser, D. 2015. The Scandinavian Caledonides: main features, conceptual advances and critical questions. *Geological Society London Special Publications*, 390, 9-43.
- Drake, H., Åström, M.E., Heim, C., Broman, C., Åström, J., Whitehouse, M., Ivarsson, M., Siljeström, S., Sjövall, P. 2015. Extreme ¹³C depletion of carbonates formed during oxidation of biogenic methane in fractured granite. *Nature Communications*, 6, 7020.
- Drake, H., Roberts, N.M.W., Heim, C., Whitehouse, M.J., Siljeström, S., Kooijman, E., Broman, C., Ivarsson, M., Åström, M.E. 2019. Timing and origin of natural gas accumulation in the Siljan impact structure, Sweden. *Nature Communications*, 10, 4736.
- Ebbestad, J.O.R., Högström, A.E.S. 2007. Ordovician of the Siljan District, Sweden. In: Ebbestad, J.O.R., Wickström, L.M., Högström, A.E.S (eds), *Rapporter och meddelanden 128: WOGOGO 2007 9th meeting of the Working Group on Ordovician Geology of Baltoscandia*. Sveriges Geologiska Undersökning, 7-26.
- Fredén, C. (ed) 1994. *Geology*. National Atlas of Sweden. SNA, Stockholm.
- Gold, T., Soter, S. 1980. The Deep-Earth-Gas Hypothesis. *Scientific American*, 242, 154–161.

-
- Hode, T., Von Dalgigk, I., Broman, C. 2003. A hydrothermal system associated with the Siljan impact structure, Sweden – Implications for the search for fossil life on Mars. *Astrobiology*, 3(2), 271-289.
- Hu, G., Dam-Johansen, K., Wedel, S., Hansen, J.P. 2006. Decomposition and oxidation of pyrite. *Progress in Energy and Combustion Science*, 32(3), 295-314.
- Johannsson, Å. 1984. Geochemical studies on the Boda Pb-Zn deposit in the Siljan astrobleme, central Sweden. *Geologiska Föreningen i Stockholm Förhandlingar*, 106(1), 15-25.
- Kenkmann, T., von Dalwigk, I. 2000. Radial transpression ridges: A new structural feature of complex impact craters. *Meteoritics & Planetary Science*, 35, 1189-1201.
- Kietäväinen, R., Purkamo, L. 2015. The origin, course, and cycling of methane in deep crystalline rock biosphere. *Frontiers in Microbiology*, 6, 725.
- Kleine, B.I., Skelton, A.D.L., Huet, B., Pitcairn, I.K., 2014. Preservation of blueschist-facies minerals along a shear zone by coupled metasomatism and fast-flowing CO₂-bearing fluids. *Journal of Petrology*, 55(10), 1905-1939.
- Komor, S.C., Valley, J.W., Brown, P.E. 1988. Fluid-inclusion evidence for impact heating at the Siljan Ring, Sweden. *Geology*, 16, 711-715.
- Lan-Feng, F., Saulwood, L., Chieh-Wei, H., Yi-Ting, T., Tsanyao, F.Y., Kuo-Ming, H. 2018. Formation and preservation of authigenic pyrite in the methane dominated environment. *Deep Sea Research Part I: Oceanographic Research Papers*, 138, 60-71.
- Lenhert, O., Meinhold, G., Arslan, A., Ebbestad, J.O.R., Calner, M. 2013. Ordovician stratigraphy and sedimentary facies of the Stumnsnäs 1 core from the southern Siljan Ring, central Sweden. *Geologiska Föreningen i Stockholm Förhandlingar*, 135, 204–212.
- McCollom, T.M., Sherwood Lollar, B., Lacrampe-Couloume, G., Seewald, J.S. 2010. The influence of carbon source on abiotic organic synthesis and carbon isotope fractionation under hydrothermal conditions. *Geochimica et Cosmochimica Acta*, 74, 2717-2740.
- McMahon, S., Hood, A., Parnell, J., Bowden, S. 2018. Reduction spheroids preserve a uranium isotope record of the ancient deep continental biosphere. *Nature Communications*, 9, 4505.
- Naumov, M.V. 2005. Principal features of impact-generated hydrothermal circulation systems: mineralogical and geochemical evidence. *Geofluids*, 5, 165-184.
- Reimold, W.U., Kelley, S.P., Sherlock, S.C., Henkel, H., Koeberl, C. 2005. Laser argon dating of melt breccias from the Siljan impact structure, Sweden: Implications for a possible relationship to Late Devonian extinction events. *Meteoritics & Planetary Science*, 40(4), 591-607.
- Schmitz, B., Yin, Q.Z., Sanborn, M.E., Tassinari, M., Caplan, C.E., Huss, G.R. 2016. A new type of solar-system material recovered from Ordovician marine limestone. *Nature Communications*, 7, 11851.
- SGU, 2023. Kartvisaren Berggrund 1:50,000 – 1:250,000. Sveriges Geologiska Undersökning. Webpage <https://apps.sgu.se/kartvisare/kartvisare-berg-50-250-tusen.html>. Accessed 2023-12-01.
- van der Plas, L., Tobin, A.C. 1965. A chart for judging the reliability of point counting results. *American Journal of Science*, 263(1), 87-90.

von Dalwigk, I. 2004. Fracture pattern in a complex impact structure - what can it tell us about crater collapse? A new look at the Siljan Impact structure. Session 5: Geology of Impact Structures, Geologiska Föreningen i Stockholm Förhandlingar, 126(1), 52-56.

Whiticar, M.J. 1999. Carbon and hydrogen isotope systematics of bacterial formation and oxidation of methane. *Chemical Geology*, 161, 291–314.

Winter, J.D. 2014. *Principles of Igneous and Metamorphic Petrology* (2nd edition). Pearson Education Limited, Harlow, UK.